

## Pairwise interactions between deformable drops in free shear at finite inertia

Peter Ojo Olapade, Rajesh Kumar Singh, and Kausik Sarkar<sup>a)</sup>

*Department of Mechanical Engineering, University of Delaware, Newark, Delaware 19716, USA*

(Received 21 December 2008; accepted 13 May 2009; published online 15 June 2009)

Interactions between a pair of equal-size viscous drops in shear are numerically investigated at finite Reynolds number ( $Re=0.1-10$ ). At low Reynolds number the simulation compares well with a previous experimental observation. Apart from the usual pairwise motion where drops driven by shear pass over each other (type I trajectory), finite inertia introduces a new type (type II) of reversed trajectory where drops approaching each other reverse their initial trajectories. The new trajectory is explained by a reversed streamline pattern observed around a single drop in an imposed shear, and is similar to what is also observed for rigid spheres at finite inertia. However, drop deformability introduces a nonuniform transition from one to the other type of trajectory—drops display type I trajectory for high and low capillary numbers and type II for intermediate capillary numbers. The phenomenon is explained by noting that increasing capillary number gives rise to competing effects—while it increases drop deformation and therefore increases resistance to sliding motion, it also increases drop flexibility, decreases inclination angle, and overall effect of the drop's presence is reduced, all helping them to slide by. The nonuniform behavior—type II trajectory for an intermediate range of capillary numbers—occurs only at Reynolds number above a critical value. Further increase in Reynolds number increases the range of capillary numbers for type II trajectory. For type I trajectory, terminal cross-stream separation increases linearly with increasing inertia indicating an enhanced shear induced diffusion. Increasing initial streamwise separation aids in reversed (type II) trajectory due to increased overlap with the reversed streamline zone. Increasing cross-stream distance expectedly facilitates (type I) sliding motion. For passing drops (type I trajectory), terminal cross-stream separation is not appreciably affected by capillary number and initial drop separation. © 2009 American Institute of Physics. [DOI: 10.1063/1.3153905]

### I. INTRODUCTION

Due to the slow velocity and small drop radius often encountered in many emulsions, inertialess Stokes analysis dominated the field of emulsion study. However, there are many applications where inertial effects even at the individual drop scale cannot be ignored. We have recently found that inertia with small values of particle Reynolds number ( $Re \sim 1-10$ ) significantly affects the dynamics of individual drops<sup>1-5</sup> and consequently their emulsion rheology.<sup>4,6,7</sup> In the case of a dilute emulsion, the single drop behavior completely determines the rheological response of an emulsion at  $O(c)$  ( $c$  is the volume fraction of drops). Concentrated emulsions, where interaction between drops cannot be neglected, are a difficult problem amenable only to careful experiments and large-scale simulations. Pairwise interaction between two drops in a shear, still a complex moving boundary value problem, leads to an  $O(c^2)$  contribution to the overall rheology.<sup>8,9</sup> It also offers useful insight into the overall response of a concentrated emulsion. In this paper we numerically investigate how inertia affects the trajectories of deformable particle pairs. We find that the drops, along with the common trajectory (type I), where they pass over each other, also display a new reversed trajectories (type II) due to finite

inertia effects, where approaching each other they reverse their motion.

The corresponding problem of pairwise interactions between rigid spheres in shear was investigated by many in the Stokes limit. Batchelor and Green<sup>8</sup> showed that for force-and-couple free spheres, trajectory of one sphere relative to the other can be open or closed in Stokes flow. In an open trajectory, particles separate after driven to contact by shear. However, for certain positions of the spheres, they orbit around each other in closed trajectories in agreement with the experimental observations by Darabener and Mason.<sup>10</sup> This result is intimately related to the existence of a region of closed streamlines around a freely rotating sphere or cylinder in a shear flow. The closed streamline region results in impeded heat and mass transfer even at large Peclet numbers.<sup>11,12</sup> Recently, effects of inertia on the flow field around rigid spheres and cylinders were investigated using analysis<sup>13,14</sup> and numerical (finite element and lattice Boltzmann) methods.<sup>15</sup> The Stokes flow results are caused by the linearity of the Stokes equation and the corresponding reversible nature of the flow field. For the same reason, in absence of inertia, surface roughness, electrostatic repulsion, Brownian motion, and other nonhydrodynamic effects, two colliding rigid spheres in a shear will return to their original streamlines. Consequently, two-sphere interactions are insufficient to account for the shear induced diffusion,<sup>16</sup> and at

<sup>a)</sup>Electronic mail: sarkar@udel.edu.

least a third sphere is needed for a qualitative explanation.

The situation, however, changes for colliding deformable drops where interactions between two drops in a shear lead to an increase in the cross-flow separation of their centers.<sup>17-20</sup> In one of the early experiments, Mackay and Mason<sup>17</sup> showed this phenomenon for quasispherical drops. More recently, numerical simulation using boundary element method<sup>18,20</sup> investigated the same phenomena in two<sup>20</sup> and three dimensions.<sup>19</sup> On the recent experimental side, observations using computer assisted video optical microscopy by Guido and Simeone<sup>21</sup> agreed quite well with past experiments and boundary element simulations. They showed that the deformation and shear stress contributions of the drops are maximal when the drops are pressed together along the compressional quadrant of the shear flow and minimal when they are drawn apart along the extensional axis; this breaks the reversal symmetry. Loewenberg and Hinch<sup>19</sup> showed that the resulting self-diffusivity is a strong function of viscosity ratio and only a moderate function of capillary number. While boundary element method is extremely suitable for computations of multiple drops, it is restricted to Newtonian Stokes flow. Effects of finite inertia on pairwise interactions between drops in a shear have not been investigated previously. For a single drop, we have recently discovered that inertia leads to a resonance phenomena<sup>1-3,22</sup> in time periodic flows with drastic effects on emulsion rheology.<sup>4,6</sup> Specifically in shear, we observed that inertia increases drop inclination angle in shear leading to a sign change in normal stresses of a dilute emulsion.<sup>7</sup> Such effects indicate that inertia would significantly affect pairwise interactions between drops in a shear.

In this respect, we note that a numerical simulation using the lattice Boltzmann method has shown that inertia results in drastic changes in pair trajectories for freely rotating rigid particles in shear.<sup>23,24</sup> The close trajectories of Stokes flow disappear, and spiraling and reversed trajectories are discovered, the latter being very similar to the ones found in the present paper. These phenomena results from the loss of fore-aft symmetry of the streamlines around a single particle in shear, which shows zones of reversed streamlines upstream and downstream of the particle as well as streamlines spiraling around it.<sup>13,15</sup> The velocity field underlying these streamlines have been computed using a singular perturbation method almost 40 years ago.<sup>25</sup> Apart from inertia, confinement (presence of wall) also affects pair trajectories. Zurita-Gotor *et al.*<sup>26</sup> showed that in Stokes flow it results in a zone of reversed streamlines and swapping trajectories due to reflection from the wall leading to cross-streamline migration and a large self-diffusivity.<sup>27</sup> In presence of inertia confinement also leads to limit cycles and fixed points due to interactions with periodic images in a simulation with periodic boundaries.<sup>28</sup> For a pair of capsules enclosed by a neo-Hookean membrane in shear, recent finite inertia computation also showed reversed trajectories (due again to the reversed streamlines around a single capsule), fixed orbits and spiraling motions, the latter two resulting from the periodic boundary conditions and the vertical confinement.<sup>29</sup> The corresponding Stokes flow computation for capsules using

boundary element does not show any reversed trajectory, fixed orbits or spiraling motion.<sup>30,31</sup>

In this paper, we study the trajectories of a pair of viscous drops at finite inertia in an unbounded shear. We use a front-tracking finite difference method<sup>32</sup> to numerically simulate the problem. We perform a careful investigation of the effects of grid resolution and domain size to eliminate the effects of boundaries. We compare with experimental results of Guido and Simeone.<sup>21</sup> The mathematical formulation and the numerical method are briefly described in Secs. II and III. In Sec. IV, we investigate in detail the effects of variation in Reynolds number, capillary number and initial drop configuration. Section V summarizes the work.

## II. GOVERNING EQUATIONS

We consider a single-fluid formulation in the entire domain, consisting of the suspended drops and the continuous matrix. The governing mass and momentum equations are

$$\nabla \cdot \mathbf{u} = 0, \quad (1)$$

$$\frac{\partial(\rho\mathbf{u})}{\partial t} + \nabla \cdot (\rho\mathbf{u}\mathbf{u}) = -\nabla p + \nabla \cdot [\mu \nabla \mathbf{u} + (\mu \nabla \mathbf{u})^T] - \int_{\partial B} d\mathbf{x}_B \kappa \mathbf{n} \Gamma \delta(\mathbf{x} - \mathbf{x}_B), \quad (2)$$

where  $\rho$  is the fluid density,  $p$  is the pressure, and  $\mu$  is the viscosity.  $\Gamma$  is the interfacial tension (assumed constant and spatially homogeneous, therefore no Marangoni effects).  $\partial B$  is the surface of drops consisting of points  $\mathbf{x}_B$ ,  $\kappa$  is the local curvature, and  $\mathbf{n}$  is the outward unit vector normal to  $\partial B$ .  $\delta(\mathbf{x} - \mathbf{x}_B)$  the three-dimensional Dirac delta function. The surface tension force, which produces a jump in the normal traction across the interface, is expressed as a singular body force. The interface moves with the fluid. Material properties, such as density and viscosity are treated as field functions of position that could undergo step changes across the interfaces. However, in this work we restrict ourselves to the viscosity-and-density matched case in the interest of brevity.

## III. NUMERICAL IMPLEMENTATION

We put two drops of radius  $a$  in a computational box (Fig. 1). For all simulations, except when we investigate the effects of initial configuration, the drop centers are initially separated by  $2.5a$  ( $\Delta x_0/a=2.5$ ) along the flow direction and  $0.25a$  ( $\Delta y_0/a=0.25$ ) along the velocity gradient direction. They are in the same  $z$ -plane (vorticity direction). One drop is placed along the centerline (not necessarily at the center) of the computational domain, and the other is placed displaced upstream and upward relative to the first one. The exact  $x$ -(streamwise) positions are chosen so that the drops are away from the boundary and separated by a specified streamwise distance  $\Delta x_0/a$ . Periodic boundary conditions are imposed along the  $x$  (velocity) and  $z$  (vorticity) directions. The upper wall of the domain moves to the right with velocity  $U$  and the lower wall moves to the left with velocity  $-U$ , thereby generating a simple shear of magnitude  $\dot{\gamma}$ . The walls are ensured to be sufficiently far away from the drops so that

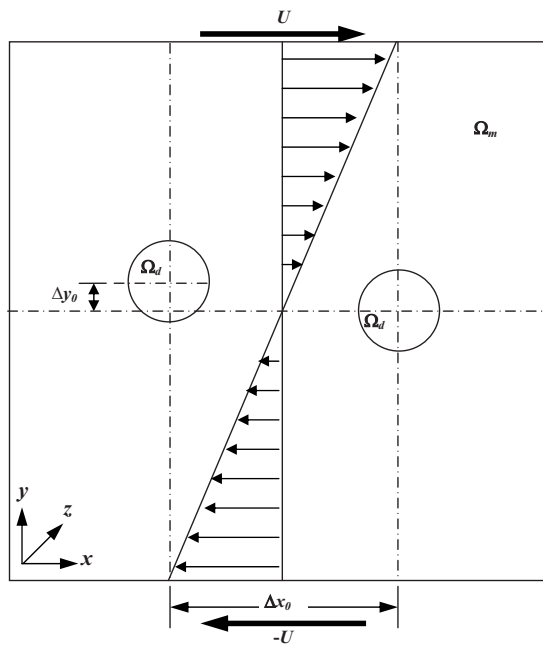


FIG. 1. A Schematic of the computational flow domain showing the initial position of the two interacting drops.

drops experience a pure shear and not a parallel channel flow of known width (see Sec. IV A on domain convergence). The initial condition of the problem is two spherical drops of radius  $a$  suddenly introduced in a shear flow.

The conservation Eqs. (1) and (2) are solved using a front-tracking finite difference method.<sup>32,33</sup> Because the method has been described in previous publications,<sup>3,5</sup> here we only provide a brief description. The method allows the entire flow to be treated as a single phase. The surface tension force appears distributed smoothly over a thin interfacial layer (four grid points). The resulting equations are solved on a fixed rectangular grid. However the interface (front) is retained in a discrete representation using flat triangles. At each time step forces due to surface tension from this discretized front is distributed on the fixed rectangular grid. A projection method is used to solve the single phase flow problem. The velocity determined on the fixed rectangular grid is interpolated to the front grid to find the velocity of the front vertices, which is used to move the front to a new location. An adaptive front regridding scheme is used to prevent excessive distortion of the front elements. The above explicit scheme suffers from the restrictions on time steps at low Reynolds number ( $\Delta t < 0.25(\Delta x)^2 \rho / \mu$ ). To overcome this restriction, we treat some of the diffusive terms implicitly in alternate spatial directions (ADI). The ADI scheme reduces the time step by one order of magnitude. We also adhere to other criteria  $\Delta t < 2.0\mu / (\rho U_{\max}^2)$  and  $\Delta t < \Delta x / U_{\max}$  at high Reynolds numbers to ensure overall convergence of our simulations.

Using the initial drop radius  $a$  as the characteristic length scale and the inverse strain rate  $\dot{\gamma}^{-1}$  as the characteristic time scale, we obtain a number of nondimensional parameters for the problem: Reynolds number  $Re = \rho_m \dot{\gamma} a^2 / \mu_m$ , capillary number  $Ca = \mu_m \dot{\gamma} a / \Gamma$ , viscosity ratio  $\lambda = \mu_d / \mu_m$ , density ratio  $\lambda_\rho = \rho_d / \rho_m$  initial configuration parameters  $\Delta x_0 / a$  and  $\Delta y_0 / a$ .

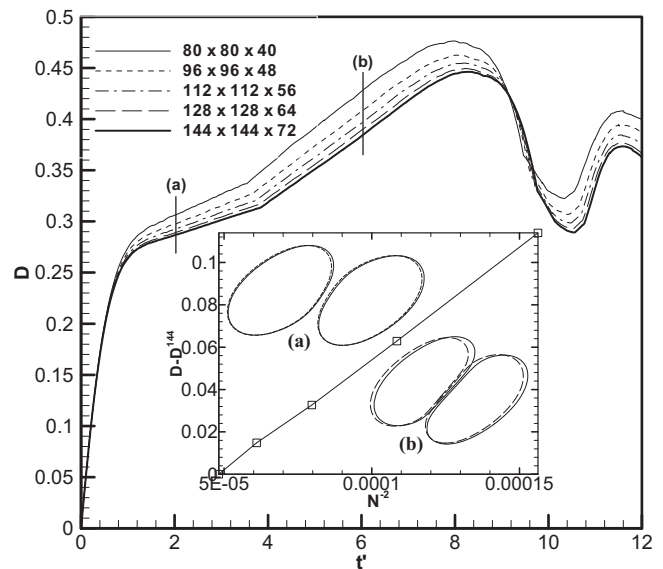


FIG. 2. Drop deformation at  $Re=2$  and  $Ca=0.2$ , for different mesh resolutions. Inset shows the error in  $D$  with reference to the  $D$  value at mesh resolution of  $144 \times 144 \times 72$  plotted against resolution ( $N$  is grid points in the  $x$  direction) at the instant corresponding to  $b$ . The actual drop shapes for the grid used in most simulations ( $96 \times 96 \times 48$ ) and that at  $144 \times 144 \times 72$  at time instants  $a$  and  $b$ .

Subscripts  $m$  and  $d$  relate to matrix and the drop phases. We restrict the present study to  $\lambda = \lambda_\rho = 1.0$ .

## IV. RESULTS AND DISCUSSION

In this section, we present the results of our numerical simulation of two drops in steady shear. As mentioned before, we study hydrodynamic interaction between two drops by placing two spherical drops of the same size in a computational domain of size  $L_x = 40a$ ,  $L_y = 10a$ , and  $L_z = 5a$ . Figure 1 shows a schematic representation of the computational domain. In this paper, we characterize deformation of a drop by the criterion  $D$  defined by Taylor<sup>34,35</sup> as  $D = (L - B) / (L + B)$ , where  $L$  and  $B$  are the maximum and minimum distances of the drop interface from its center.

### A. Grid and domain size convergence

For a single drop in shear and other flows, convergence of our computational method has been carefully investigated before.<sup>22</sup> Figure 2 investigates convergence for the two-drop case in a  $10a \times 10a \times 5a$  domain. The drop deformation (both drops experience the same deformation as discussed below) converges as we increase the discretization level from  $80 \times 80 \times 40$  to a maximum of  $144 \times 144 \times 72$ . We choose grid level  $96 \times 96 \times 48$  for our simulation. Although we notice a slight deviation in the value of  $D$  at this grid level, the actual drop shape does not change significantly from that at  $144 \times 144 \times 72$ . They are shown for the grid level used in the simulation and the maximum level for two different time instants [(a) and (b) inside the inset] during the interaction between drops. We do notice that the drop motions from two-discretization levels are slightly different at the latter instant (b) where the drop experiences larger deformation. However, we consider such discrepancies within the accept-

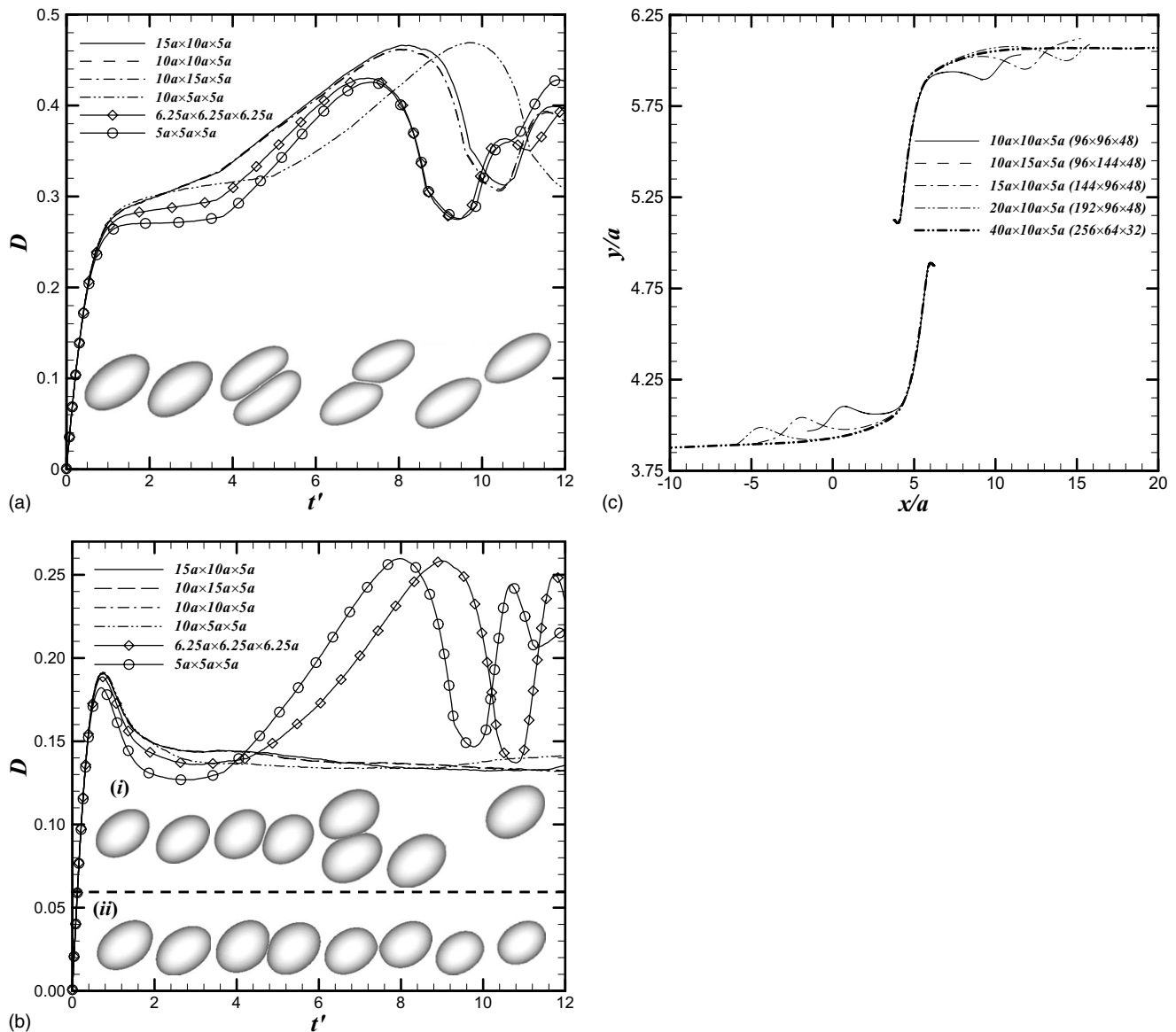


FIG. 3. Plot of deformation vs time at  $\Delta x_0/a=2.50$ ,  $\Delta y_0/a=0.25$ , for different computational domain sizes: (a) for  $Re=2$ ,  $Ca=0.2$ ; drop shapes for  $10a \times 10a \times 5a$  in the inset, (b) for  $Re=3$  and  $Ca=0.1$ ; drop shapes for  $6.25a \times 6.25a \times 6.25a$  in inset (i) and for  $10a \times 10a \times 5a$  in inset (ii). (c) Trajectory for different domain sizes at  $Re=2$ ,  $Ca=0.20$ ,  $\Delta x_0/a=2.50$ , and  $\Delta y_0/a=0.25$  show the effect of periodic boundary condition.

able limits. For this time instant, the deformation shows quadratic convergence with discretization (inset of Fig. 2). We also note that one has to be careful for long-time simulation results, when due to domain periodicity the drops may computationally come close to each other after passing each other. Below we investigate this issue.

We investigate the effects of domain size on our computation [Figs. 3(a)–3(c)]. As we will see below, drop trajectories at finite inertia are of two types similar to what is observed for rigid particle pairs.<sup>23</sup> One is where the drops are able to slide past each other as in Stokes flow, and the deformation evolution takes the form shown in Fig. 3(a) simulated at  $Re=2$  and  $Ca=0.2$  (the inset shows the drop shapes evolution at four time instants). For other values of parameters, drops follow a reversed trajectory. In Fig. 3(b) we show the deformation for such a case at  $Re=3.0$ , and  $Ca=0.1$ . However we note that with smaller domain sizes, the drops actu-

ally slide past each other [drop shapes with  $6.25a \times 6.25a \times 6.25a$  domain size are shown in inset (i) of Fig. 3(b)]. Moreover only for four larger domain sizes we get the correct trajectories [inset (ii) of Fig. 3(b)]. This emphasizes the importance of choosing a sufficiently large domain. Two types of trajectories give rise to very different deformation evolution. A domain size of  $10a \times 10a \times 5a$  is found adequate for distinguishing the trajectory type. The fact that domain size affects results was noted by Ref. 29, which used a cubic computational domain of size  $6.25a \times 6.25a \times 6.25a$ .

As noted above one needs to make sure that after the drops separate they do not come close to the upstream and downstream boundaries of the domain—it would otherwise lead to their periodic interaction. Indeed, plotting drop trajectories in a  $10a \times 10a \times 5a$  domain shows that they are affected after their postcollision separation [Fig. 3(c)]. This necessitates larger dimension in the flow direction for long-

time simulation. Long simulation is critical for predicting postcollision terminal cross-stream offset that a drop experiences giving rise to shear induced diffusion. Fortunately, we find that although the drop deformation is slightly affected by discretization [Fig. 2(a)], drop trajectories are not affected much by a coarse discretization on a longer domain. Indeed the short- and long-domain simulations share common trajectory until after collision [Fig. 3(c)]. Therefore, for computing trajectories, we use a domain size of  $40a \times 10a \times 5a$  with a discretization level of  $256 \times 64 \times 32$ . We carefully ensure that the simulated trajectory with coarser discretization but longer domain matches with that with finer discretization for the initial short time. As we see below this becomes an issue near the threshold when one type of trajectory changes to another.

Note that the left drop is in a positive imposed flow field by its placement. By a change of frame, the drops can be placed symmetrically across the central  $x-z$  plane resulting in a symmetric problem [as is seen in Fig. 3(c)]. The fact that the physical symmetry is preserved with a numerical simulation where one drop is placed nearer to a computational boundary demonstrates that the computational boundaries are far away, and the numerical implementation of imposed free shear is accurate. It also explains the same deformation experienced by both drops. We present drop trajectories in their symmetric form in the changed reference frame.

## B. Comparison with experiments of Guido and Simeone

Guido and Simeone<sup>21</sup> experimentally investigated binary collision between polydimethylsiloxane (PDMS) drops in polyisobutylene (PIB) matrix under low Reynolds number ( $Re \sim 10^{-7}$ ). A single drop was first sheared to an elongated shape, which broke into two equal-size drops offset in both cross-stream and streamwise directions, when the shear was stopped. The shear was then reapplied to initiate a binary collision. Coalescence of drops was found to be extremely rare, and happened only for PIB drops in PDMS matrix. In Figs. 4(a)–4(d), we compare our simulation with the experimental observations for the evolution of deformation, orientation angle, vertical separation, and the angle joining the drop centers. We present the drop shapes in Fig. 5 at the same time instants marked in Fig. 4. Drop deformation is determined by the local velocity gradient rather than the actual velocity, which influences the bodily motion. However as noted above, both drops being far away from the wall, interactions between them give rise to exactly the same deformation for both, as was also observed in the experiment.<sup>21</sup> We note from Figs. 4(a) and 5 that the drops increase their deformation as they approach each other, it being maximum when they are fully aligned in the compressional quadrant. At the same time, the inclination angle  $\varphi$  [Fig. 4(b) plots  $90^\circ - \varphi$  following Guido and Simeone<sup>21</sup>] also increases reaching a maximum. The inclination angle and deformation are phase shifted in that the maximum of inclination angle coincides with the maximum rate of increase of deformation. As they slide over each other, drops align more with the flow reaching a minimum [maximum in Fig. 4(b)] in inclination

angle first, and then deformation reaching a maximum. It is followed by a second lower maximum both for inclination angle and then for deformation as drops pull apart from each other in the extensional quadrant. In Fig. 4(c), we note that the drops increase their cross-stream separation after interaction indicating shear diffusive interaction between drops unlike rigid particle pairs, where particles come back to their initial cross-stream separation. In Fig. 4(d), angle between drop centers shows that changes in deformation takes place when they are passing over each other. After being fully separated, the drops regain their shape. As mentioned before, our explicit simulation method is restricted to finite inertia. However, simulation at  $Re=0.02$  shows excellent agreement with the experiments performed at  $Re \sim 10^{-7}$  for vertical separation and the angle. The deformation shows some difference at the peak value. However, note that even inertialess Boundary element solution showed slight discrepancy at the peak (Fig. 18 in Ref. 21). We conclude that the front tracking simulation tool is appropriate for the present study.

## C. Effects of Reynolds number variation

Because of the large number of parameters involved in this problem, we study a reference case with a set of representative values for some of the parameters. We take initial separations to be  $\Delta x_0/a=2.5$  and  $\Delta y_0/a=0.25$  (Guido and Simeone<sup>21</sup> noted that drops start interacting when they are two radii away) for most of our simulations except in sections where we study the effects of initial separation. We investigate three representative cases  $Ca=0.01$ ,  $Ca=0.1$ , and  $Ca=0.2$ , all below the critical capillary number for drop breakup in Stokes flow, keeping in mind that drop deformation is expected to increase with increasing Reynolds number.

For  $Ca=0.1$ , Fig. 6(a) plotting deformation as a function of time for increasing Reynolds number shows that increased inertia leads to increased deformation but otherwise similar pattern of growth and decline for  $Re=0.1, 1, 2$ , as in low Reynolds number shown in Fig. 4. The sudden increase in slope of the deformation, which marks the onset of alignment of drops with each other in the compressional quadrant of the shear flow, starts at different time  $t'$  for different  $Re$ . The time  $t'$  taken by drops to be aligned with each other increases with the increase in  $Re$  of the flow. Indeed the time to reach the peak deformation increases linearly with Reynolds number (inset). The linear increase can be understood by arguing that the flow field near a single drop can be approximated as  $\mathbf{u} \sim \mathbf{u}^{(0)} + Re \mathbf{u}^{(1)}$ ; such an expansion was obtained for the inner flow field around a rigid sphere at finite inertia using a perturbation method.<sup>14,25</sup> Each drop follows the flow field induced by the other giving rise to a linear with  $Re$  slowing down of the time scale of approach. The slowed time scale at higher  $Re$  is also a result of the fact that as the drops are compressed more at high  $Re$ , part of the fluid in the near contact region between drops is forced out of the gap. The resulting flow in the gap leads to an increase in the viscous stress in the region. This increased viscous stress also causes the drops at high  $Re$  to align relatively slowly along the compressional quadrant.

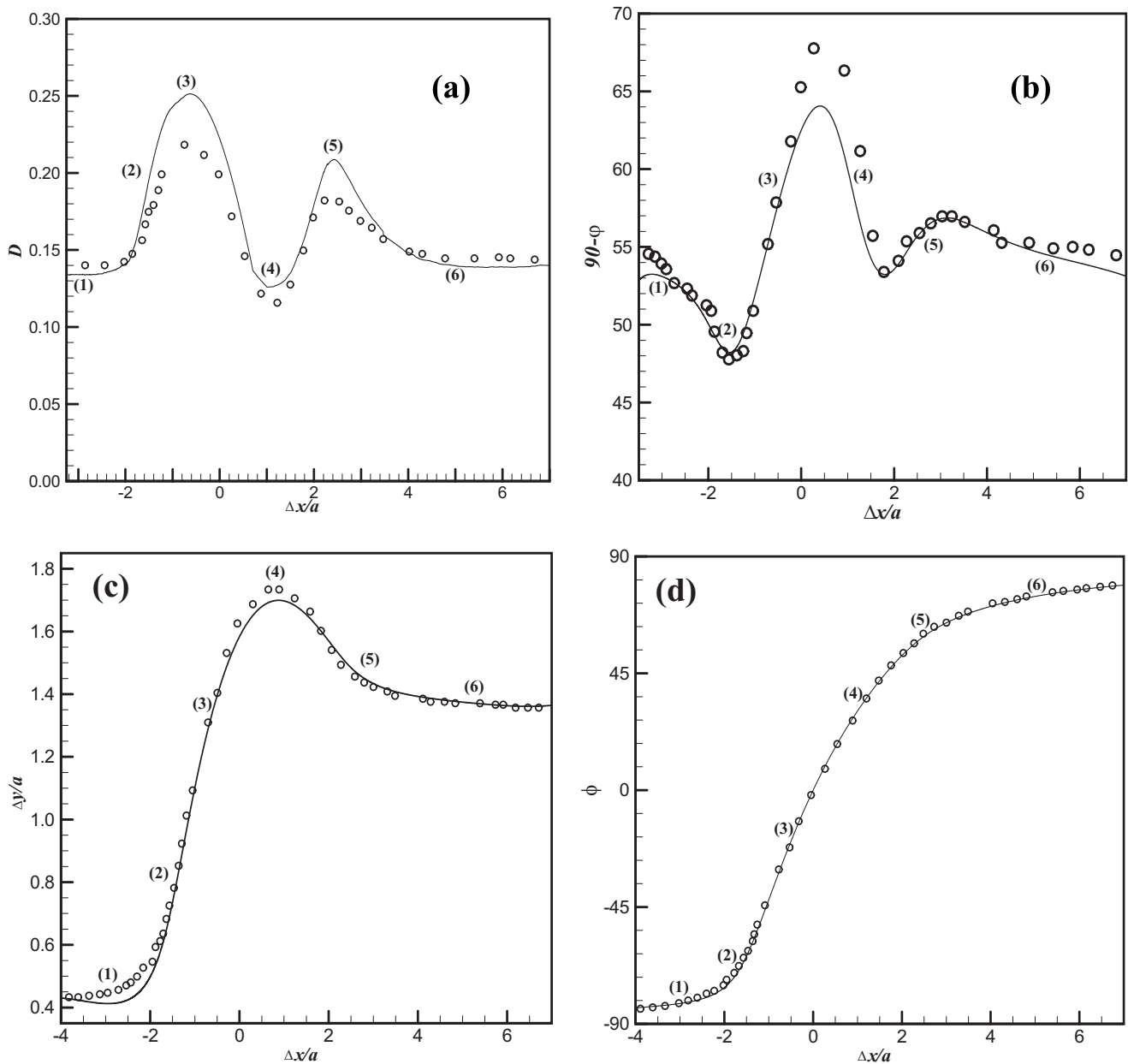


FIG. 4. Comparison of simulation and experimental results of Guido and Simeon (open circle) at  $Re=0.02$ ,  $\lambda=1.4$ ,  $Ca=0.13$ , and  $\Delta y_0/a=0.43$ : (a) deformation, (b) orientation angle, (c) relative trajectory, and (d) angle  $\phi$  the line joining the centers of the two interacting drops and the  $y$ -axis.

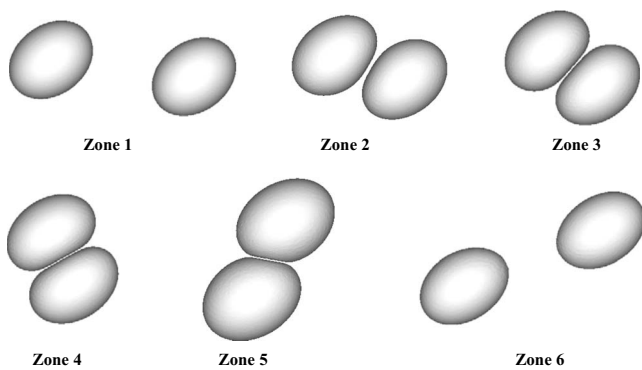


FIG. 5. Simulated images of drops at the same time instants shown in Fig. 4 for  $Re=0.02$ ,  $\lambda=1.4$ ,  $Ca=0.13$ , and  $\Delta y_0/a=0.43$ .

The underlying physics can be better explained by concurrently observing the trajectories of the drops' centers of mass in Fig. 7. We show the trajectory on a long domain as the drops take a long time to reach their terminal streamlines. For  $Re=0.1, 1, 2$ , enlarged view of the interacting part of the trajectory in the inset (because of the symmetry only the left drop was shown) shows that the drops at increased inertia translate further in the flow direction due to the larger inertia before they begin to separate vertically along the velocity gradient direction. The streamline pattern (e.g., shown in Fig. 9) near a drop at finite inertia favors a closer approach of the two before separation. We call this trajectory seen at lower Reynolds numbers ( $Re=0.1, 1, 2$ ) type I drop trajectory; it is qualitatively the same as seen in Stokes flow. We note that after separation drops recover slightly their precollision cross-stream position for the lowest Reynolds number  $Re$

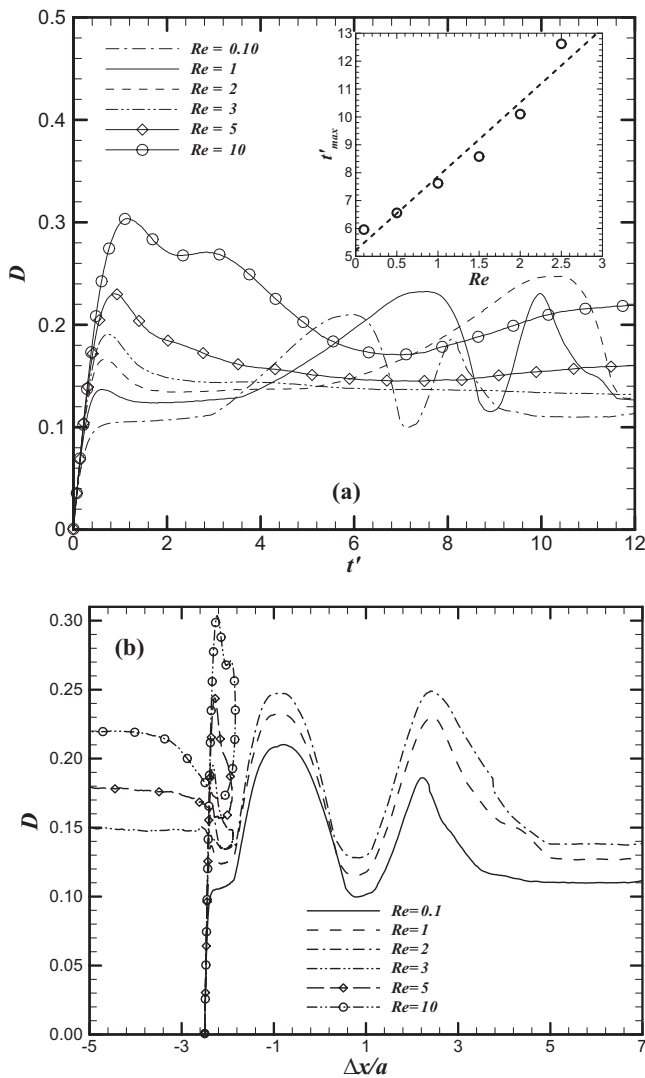


FIG. 6. plots of (a) deformation vs time (b) deformation vs  $\Delta x/a$  at  $Ca=0.1$ ,  $\Delta x_0/a=2.5$ , and  $\Delta y_0/a=0.25$  and various Reynolds numbers. Inset of (a) plots time to attend maximum deformation vs  $Re$  for type I trajectory.

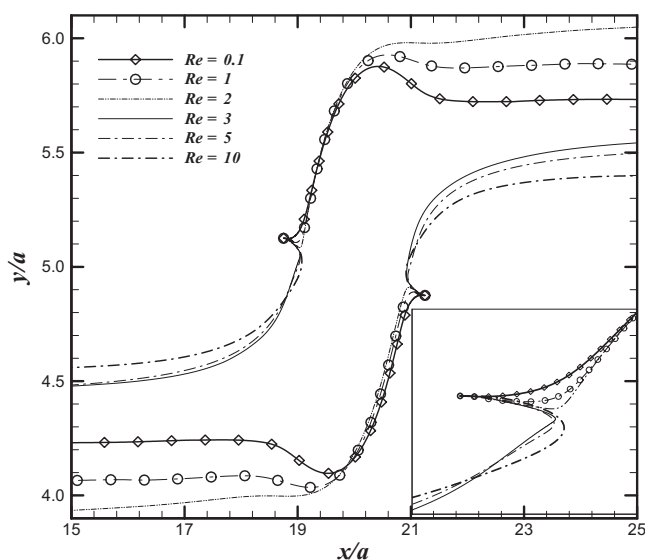


FIG. 7. Trajectories of the center of mass of the drops at  $Ca=0.1$ ,  $\Delta x_0/a=2.5$ ,  $\Delta y_0/a=0.25$  and various Reynolds numbers. The inset shows an enlarged view of the initial part of the left drop's trajectory.

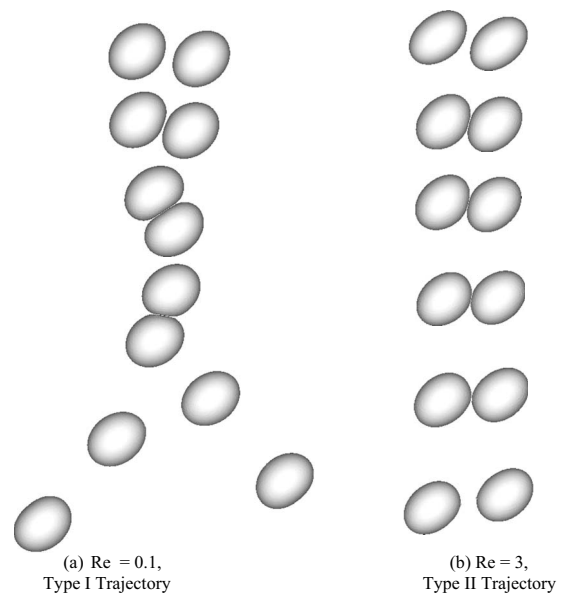


FIG. 8. Images of drops showing at  $t'=2, 4, 8, 10, 14$ , and  $16$  (top to bottom) for  $Ca=0.1$ ,  $\Delta x_0/a=2.5$ ,  $\Delta y_0/a=0.25$ , and two Reynolds numbers showing two types of trajectories.

$=0.1$ , as also seen in Fig. 4(c). With increasing Reynolds number the recovery decreases indicating larger shear induced diffusion at finite inertia.

At higher Reynolds numbers ( $Re=3, 5, 10$ ) we see a qualitative change in drop behavior. Drops are not able to slide past each other (Figs. 6 and 7). The left drop, as it approaches the other, moves downward. Likewise, the right drop moves upward. Then they follow a reversed trajectory in that they both turn back driven by the flow in their new cross-stream positions. We denote this as the type II trajectory. Drops traversing each type is shown in Fig. 8. The fundamentally new type of trajectory at higher Reynolds numbers is explained by the streamline pattern around a single drop in shear at different Reynolds number (Fig. 9). As was shown for rigid particles,<sup>14,15</sup> at finite Reynolds numbers, a region of reversed streamlines appear before and after the drop. The extent of the region increases with increasing Reynolds number. When the region extends to the position of the other drop, each drop is forced toward a reversed trajectory by the flow induced by the other. The physics is similar to that of the rigid particles.<sup>23</sup> The corresponding reversed streamlines around a single rigid sphere in shear are shown in Ref. 14 using the perturbative solution obtained in Ref. 25. However, the deformability defined by the capillary number plays a crucial role as we see below. To understand the reversed streamline pattern around the drop, one needs to focus on the motion of a fluid particle above but close to the central plane, and therefore having small  $x$ -velocity [Fig. 9(b)]. For it to go around the drop, it would have to accelerate to larger velocities of the shear away from the central plane. Unlike in Stokes flow, in presence of inertia such acceleration involves a force barrier which pushes the fluid particle below the central plane in a reversed trajectory.

On the other hand, one would expect that with higher initial cross-stream offset  $\Delta y_0/a$ , the left drop will be far

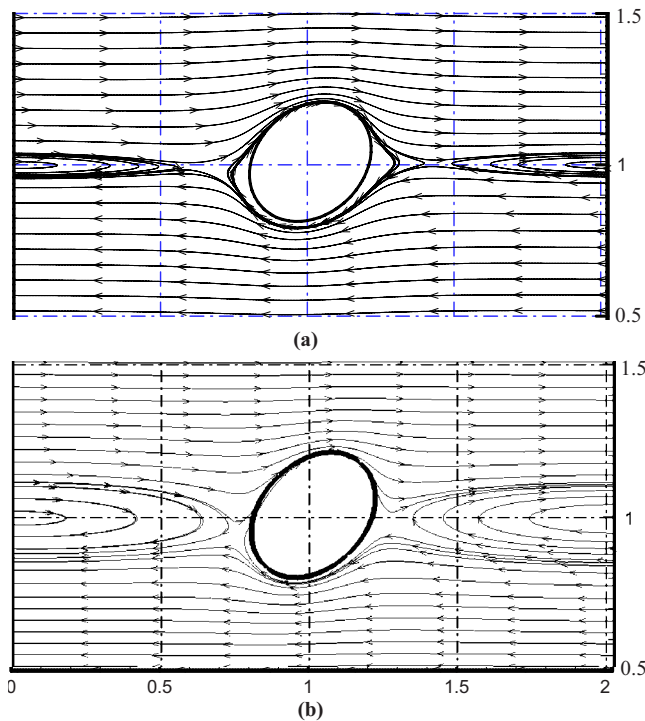


FIG. 9. (Color online) Streamlines in the central plane of the flow domain for a single drop at  $Ca=0.10$  for (a)  $Re=0.1$  and (b)  $Re=3$ .

above the zone of reversed streamlines (shown in Fig. 9) leading to drops passing each other in a type I trajectory (see Sec. IV E for effects of  $\Delta y_0/a$  and  $\Delta x_0/a$ ). Therefore, for fixed Reynolds and capillary numbers, the flow domain is divided into two distinct regions by a flow separatrix: for small initial cross-stream offset, the drop will undergo type II trajectory. For each parameter involved in the problem, one can find the threshold value that indicates a transition from one to the other type of trajectory. The exact value of the threshold, however, would sensitively depend on the numerics, and only a bound for such values can be obtained with increasingly refined numerical computation. Here we provide a qualitative view of the flow behavior (see Fig. 14 for a phase plot showing two trajectories as a function of  $Ca$  and  $Re$ ).

For each type of trajectory, deformation, inclination, and angle joining drop centers [we only show deformation in Fig. 6(b)], when plotted as a function of  $\Delta x/a$ , become similar in nature for all Reynolds numbers indicating that although increased Reynolds number increases the time scale, the effective interactions are determined by the interdrop separation.

Figure 10(a) shows the change in streamwise separation  $\Delta x/a$  between drop centers as a function of time. It increases (becomes more negative) after collision for type I (type II) trajectory. For drops sliding by each other (type I), increased inertia decreases  $\Delta x/a$  for earlier times, in conformity with our discussion of Figs. 6(a) and 7. The drop collision causes increased cross-flow separation  $\Delta y/a$ ; the drops after collision therefore have larger relative streamwise velocity than before, and so they separate faster in the  $x$ -direction.

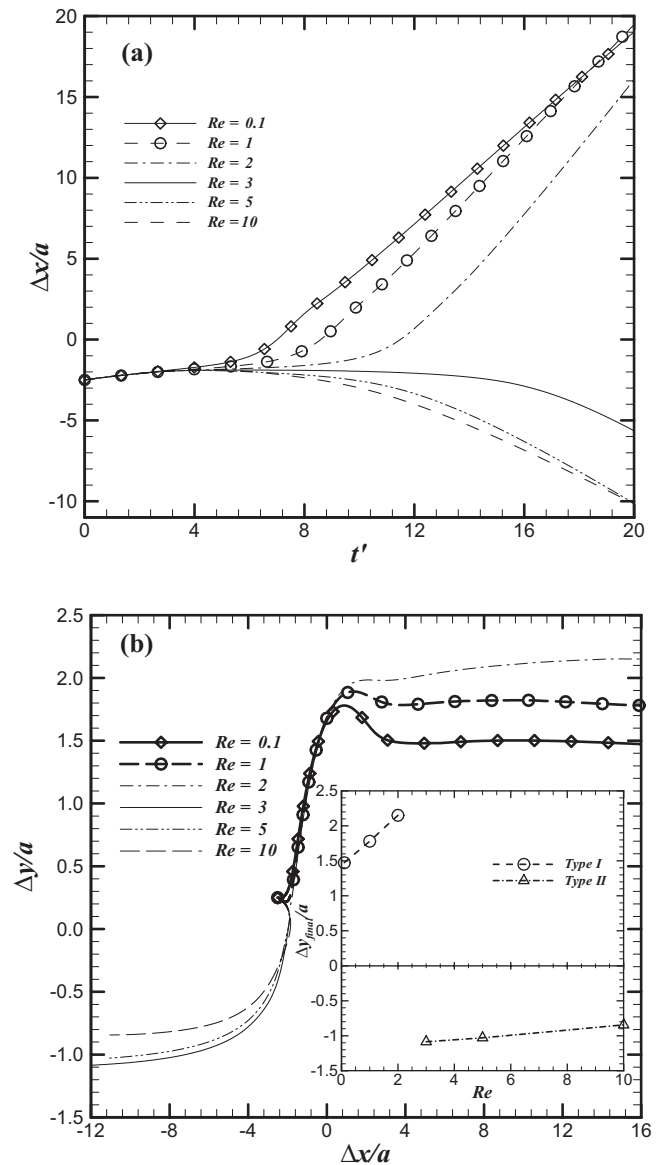


FIG. 10. Plots of (a)  $\Delta x/a$  with  $t'$ , and (b)  $\Delta y/a$  with  $\Delta x/a$ , of the two interacting drops for  $Ca=0.1$ ,  $\Delta x_0/a=2.5$ , and  $\Delta y_0/a=0.25$  at various Reynolds numbers. Inset of (b) shows terminal  $\Delta y/a$  as a function of Reynolds number.

Figure 10(b) shows the cross-flow separation  $\Delta y/a$  as a function of  $\Delta x/a$ . Note the similarity with Fig. 7. The net lateral displacement increases almost immediately at  $Re=0.1$  while, in case of  $Re=1$  and 2, it first decreases slightly before it begins to increase indicating a slight downward motion of the left drop and slight upward motion of the right drop (also see Fig. 7). The post collision vertical separation increases with increased inertia. The tendency of the left drop to follow its original streamline can still be seen at  $Re=0.1$ . For higher Reynolds numbers ( $Re=3, 5, 10$ )  $\Delta y/a$  is negative because of type II trajectory. The terminal  $\Delta y/a$  plotted as a function of Reynolds number shows a linear increase for both types of trajectories.

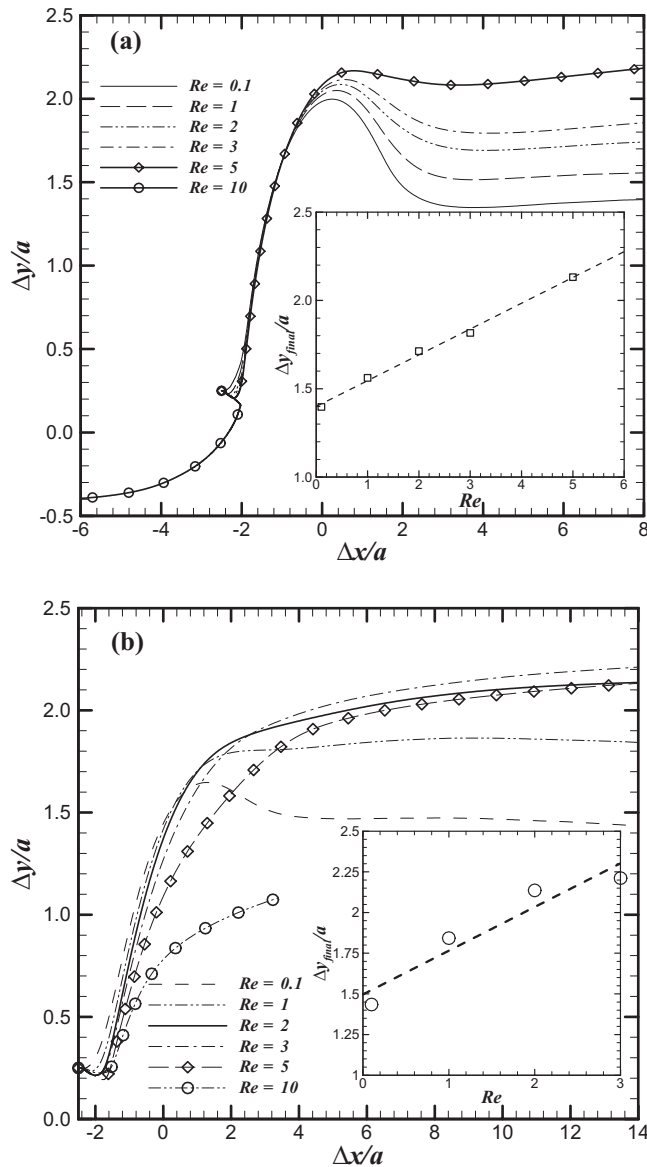


FIG. 11. Cross-stream offset  $\Delta y/a$  as a function of time for  $\Delta x_0/a=2.5$ ,  $\Delta y_0/a=0.25$  and various Reynolds numbers for (a)  $Ca=0.01$  (b)  $Ca=0.20$ . Inset shows its terminal value as a function of Reynolds number.

#### D. Effects of capillary number variation at finite inertia

In Figs. 11(a) and 11(b), we plot vertical separation  $\Delta y/a$  as a function of  $\Delta x/a$  for the same parameter values as Fig. 10(b) except at  $Ca=0.01$  and  $0.2$  (insets show final cross-stream offset varies linearly with  $Re$ ). At  $Ca=0.01$  type II trajectory seen in Fig. 6(b) for  $Re=3$  and  $Re=5$  at  $Ca=0.1$  change to type I. Only for  $Re=10$ , we notice type II trajectory (a coarse discretization of  $256 \times 64 \times 32$  in a  $40a \times 10a \times 5a$  domain leads erroneously to a type I trajectory for this parameter; we use a finer discretization for this case). For  $Ca=0.2$ , we see type I trajectory for all Reynolds numbers investigated. At the high end,  $Re=5$  and  $10$ , drops deform excessively in the compressional quadrant ( $D > 0.6$ , not shown here) leading to eventual breakup of the drops. We therefore see an unusual phenomenon: type I trajectory at  $Ca=0.01$  [Fig. 11(a)] and  $Ca=0.2$  [Fig. 11(b)] for  $Re=3$  but type II for  $Ca=0.1$  [Fig. 6(b)].

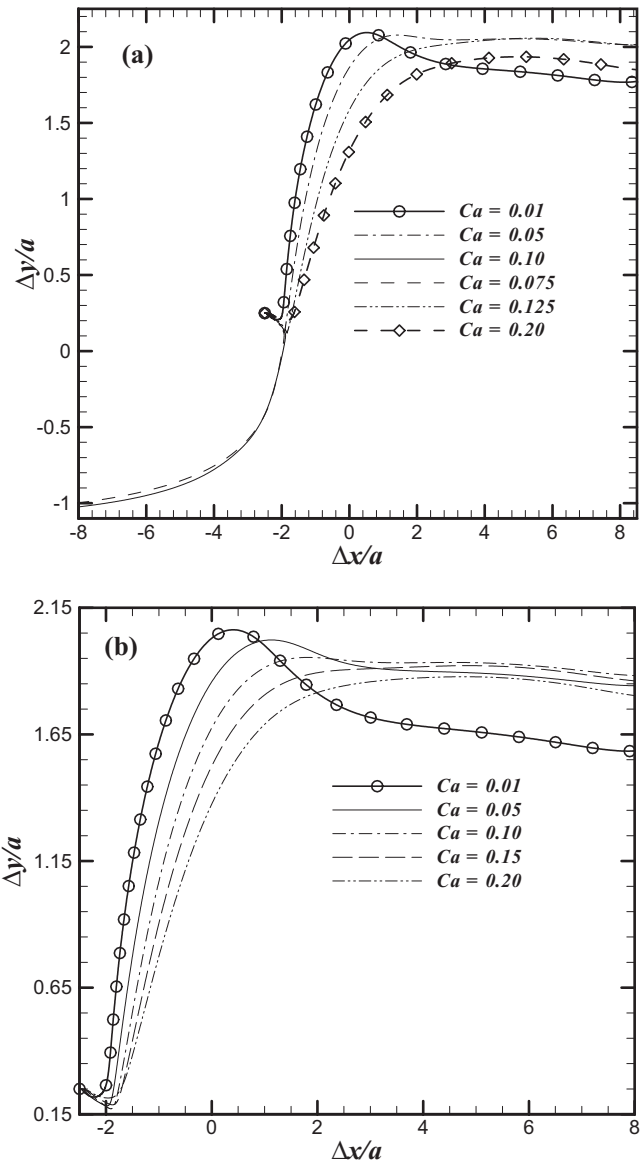


FIG. 12. Cross-stream offset  $\Delta y/a$  as a function of time at (a)  $Re=3$ ,  $\Delta x_0/a=2.5$  and  $\Delta y_0/a=0.25$ , (b)  $Re=2$ ,  $\Delta x_0/a=2.5$ , and  $\Delta y_0/a=0.25$  for various  $Ca$  values.

In Fig. 12(a) the effects of capillary number variation for the case of  $Re=3$  is investigated further. We notice a “non-uniform” behavior change with  $Ca$ , in that for smaller  $Ca$  ( $Ca=0.01, 0.05$ ) drops are able to pass each other (type I); as the  $Ca$  is increased to an intermediate range ( $Ca=0.07, 0.1$ ), drops follow reversed trajectories (type II), and then upon further increase of  $Ca$  drops again pass each other (type I). The results are verified by simulations at higher resolution.

To investigate the cause of the type II trajectory for intermediate  $Ca$  values, we plot streamlines around a single drop in steady shear at three capillary numbers ( $Ca = 0.01, 0.1, 0.2$ ) when the drop reaches a steady shape in Fig. 13. We notice that the drop progressively deforms more with increased capillary number as expected. It aligns substantially more with the flow at the highest capillary number ( $Ca=0.2$ ), which would facilitate drops to slide by each other.<sup>19–21</sup> We also note that the streamline patterns and the reversed flow zone do not show significant change with in-

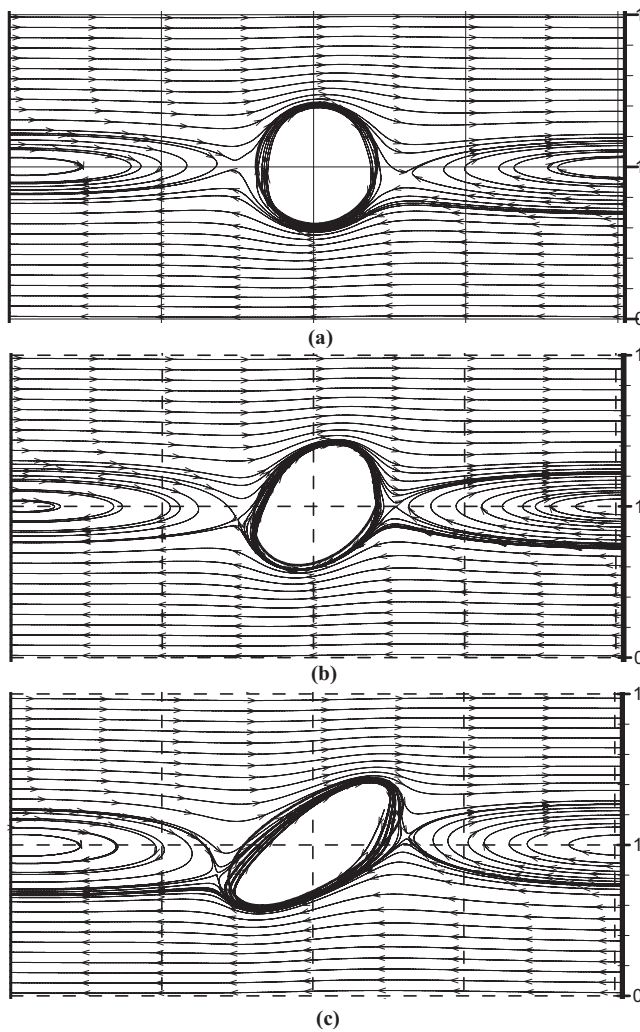


FIG. 13. Streamlines at the central plane of the flow domain for a single drop at  $Re=3$  for (a)  $Ca=0.01$ , (b)  $Ca=0.1$ , and (c)  $Ca=0.20$ .

creasing capillary number from  $Ca=0.01$  to  $Ca=0.1$ , but at  $Ca=0.2$ , the point marking the zone's boundary is shifted away from the central drop, which helps the upstream drop slide by. The nonuniform behavior can be explained by arguing that as  $Ca$  increases, deformation increases and part of the more deformed drop reaches the region with reversed streamline region responsible for the reversed trajectories. The larger deformation also impedes approaching drops preventing them from sliding over each other. However, increasing  $Ca$  also decreases the overall effects of the presence of the viscosity matched drops on the flow field. Drops experience less opposing force. Furthermore, a smaller inclination angle  $\varphi$  at larger  $Ca$  facilitates drops to pass by each other. Therefore there is a competition between these two effects that ultimately determines the type of trajectory.

In Fig. 12(b), we see type I trajectory for all capillary numbers at  $Re=2$ . Unlike the  $Re=3$  case, there is no intermediate range of capillary numbers where the drops follow type II trajectory, indicating that the occurrence of type II for intermediate  $Ca$  takes place only for Reynolds number above a critical value. In Fig. 14, we numerically compute the parameter ranges in  $Re$ - $Ca$  space that results in type I and II

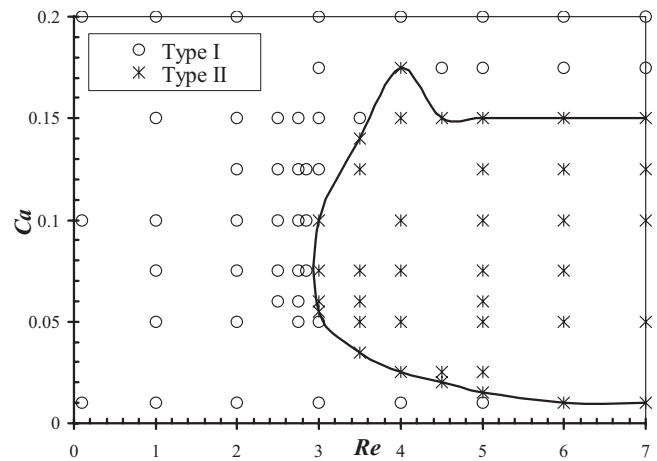


FIG. 14. Type of trajectory as a function of Reynolds number and capillary number for  $\Delta x_0/a=2.5$ ,  $\Delta y_0/a=0.25$ .

trajectories for  $\Delta x_0/a=2.5$  and  $\Delta y_0/a=0.25$ . The critical Reynolds number for a nonuniform variation with  $Ca$  is  $Re \sim 3.0$ , below which one sees type I trajectories for all  $Ca$  values. As the Reynolds number is increased above the critical value, the range of intermediate  $Ca$  values associated with type II trajectory broadens. As noted earlier, it is difficult to numerically delineate exactly the critical value for transition of a parameter. However the simulation clearly indicates the different zones. We note that the diagram depends on initial separation between drops. For instance, in contrast to Fig. 12(b),  $Re=2.0$  but  $\Delta x_0/a=2.75$  instead of  $\Delta x_0/a=2.5$  results in type I trajectories for lower ( $Ca < 0.05$ ) and higher ( $Ca > 0.175$ ) capillary numbers and type II for intermediate capillary numbers (figure not shown for brevity). Finally, we note that terminal  $\Delta y/a$  only weakly depends on  $Ca$  for drops following the type I trajectory (Fig. 12).

### E. Effects of initial separations $\Delta x_0/a$ and $\Delta y_0/a$

So far, we have studied cases with initial streamwise and cross-stream separations between drops to be  $\Delta x_0/a=2.5$  and  $\Delta y_0/a=0.25$ . In this section, we briefly investigate the effects of varying them. Admittedly for large  $\Delta y_0/a$ , drops would slide by each other in a type I trajectory. We vary  $\Delta y_0/a$  from 0 to 0.5 while fixing  $\Delta x_0/a$  at 2.5. In Fig. 15 drops show type I trajectory for  $Re=0.1$  for all  $\Delta y_0/a$ . In the inset, for a higher Reynolds number ( $Re=2.0$ ), we notice that the drop trajectories change from type I to type II for small  $\Delta y_0/a$  due to the increased overlap of drops with the reversed flow region. Note that for  $Re=0.1$ , even at  $\Delta y_0/a=0$ , the left drop flows over the right drop. A similar observation was also made by Lac *et al.*<sup>30</sup> for liquid capsules enclosed by elastic membrane colliding in shear flow in contrast to the comment made in Ref. 29. Two spherical drops placed in shear initially do not have any relative velocity due to symmetry. However slight perturbation created by the drop deformation breaks the symmetry; the resulting flow field allows the drops to pass each other. Even though the type of trajectory is determined by  $\Delta y_0/a$ , the terminal ver-

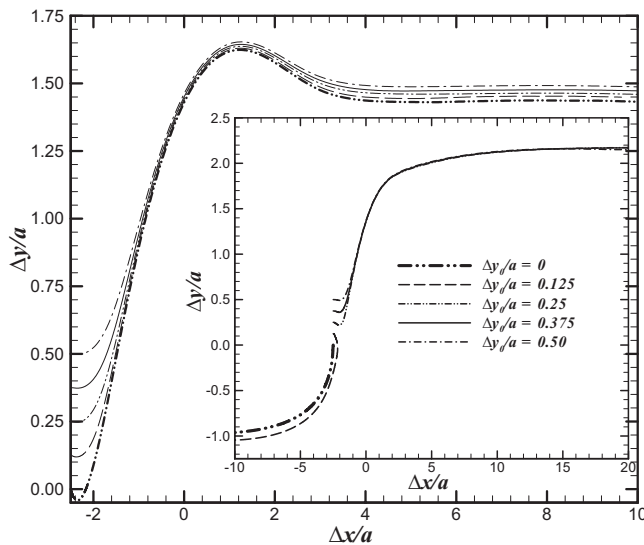


FIG. 15. : Cross-stream offset  $\Delta y/a$  as a function of time at  $Re=0.1$ ,  $Ca=0.2$ ,  $\Delta x_0/a=25$  and various  $\Delta y_0/a$  values. Inset shows the same at  $Re=2$  with identical values for other parameters.

tical offset does not vary appreciably with  $\Delta y_0/a$  when drops follow a type I trajectory.

Figure 16 investigates the effects of different  $\Delta x_0/a$  for two Reynolds numbers  $Re=0.1$  and  $2.0$  (inset). At both Reynolds numbers, type II trajectory is noticed for larger  $\Delta x_0/a$ , the critical  $\Delta x_0/a$  being higher at the lower Reynolds number. From the streamline plots around a single drop shown in Fig. 9, we note that increasing streamwise offset and Reynolds number increases the overlap of the left drop with the reversed flow region, which leads to the reversed (type II) trajectories. Terminal vertical offset remains insensitive to  $\Delta x_0/a$  for drops in type I trajectory.

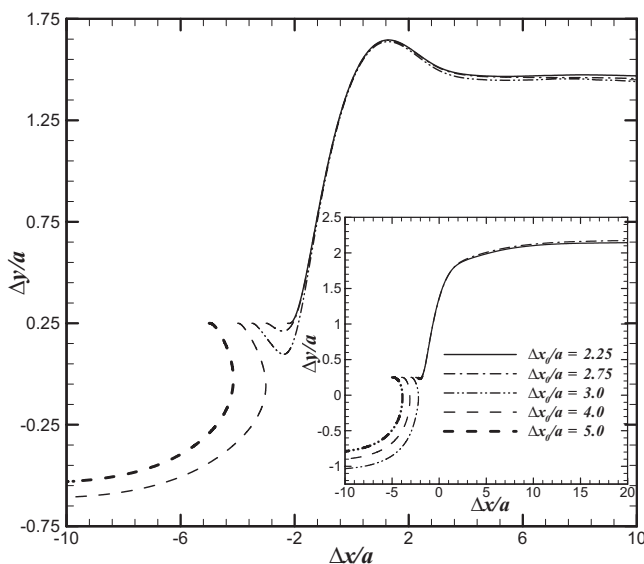


FIG. 16. Cross-stream offset  $\Delta y/a$  as a function of time at  $Re=0.1$ ,  $Ca=0.2$ ,  $\Delta y_0/a=0.25$  and various  $\Delta x_0/a$  values. Inset shows the same at  $Re=2$  with identical values for other parameters.

## V. SUMMARY

We perform a detailed numerical investigation of pair interactions between two equal-sized viscous drops in a shear flow at finite inertia. Results at small Reynolds number ( $Re=0.02$ ) match very well with experimental observations by Guido and Simeone<sup>21</sup> in predicting drop trajectory, orientation, inclination, and deformation. Larger inertia introduces a new type of reversed trajectory (type II) for drops in contrast to the usual motion of drops sliding by each other (type I) in Stokes flow. The size of the computational domain is found to be critical in obtaining the right result for the imposed free shear. Smaller domain size erroneously results in qualitatively different types of trajectories due to confinement, which was shown recently to yield different trajectories in case of rigid spheres.<sup>26</sup>

For cases displaying type I trajectory, increased inertia leads to a higher postcollision cross-stream separation which in turn results in enhanced shear induced diffusivities. The reversed trajectory would also contribute to increased diffusivity.<sup>26</sup> The terminal cross-stream separation varies linearly with Reynolds number. Although presence of both drops modifies the velocity field, an explanation of the reversed trajectory can be found in a zone of reversed streamlines around a single drop in shear; the phenomenon is very similar to what is also observed for rigid particles at finite inertia. Each drop follows the reversed streamline generated by the other. The type of trajectory is a function of Reynolds number, initial cross-stream and streamwise separations, and capillary number. Increasing Reynolds number increases the size of the region with reversed streamlines; therefore for certain fixed values of all other parameters, type I trajectory changes into type II with increased Reynolds number.

With capillary number variation, we find type I trajectory for low and high capillary numbers and type II for intermediate capillary numbers. In contrast, we note that for viscous drops, previous research found little influence of capillary number on binary collisions.<sup>19</sup> The observed transition from one type to the other for intermediate capillary numbers is due to the competing effects of decreasing interfacial force. It increases the drop deformation, increasing its overlap with the zone of reversed streamlines transitioning type I trajectory into type II for intermediate capillary numbers. However, at higher capillary numbers, a drop does not affect the flow, provides very little resistance to the other drop, and therefore once again leads to type I trajectories. The nonuniform variation (from type I to type II and back to type II for increasing capillary number) in the  $Re$ - $Ca$  phase space is seen only for Reynolds numbers larger than a critical value. The range of intermediate  $Ca$  values associated with type II trajectory increases with Reynolds number above the critical value. The phase diagram is also a function of initial separation between drops. The final cross-stream separation between passing (type I) drops is a weak function of  $Ca$ .

As expected for very large initial cross-stream separation, drops show type I trajectory. Therefore, as we increase initial cross-stream separation from very small value, drops displaying type II trajectories transition into type I. Even for zero initial cross-stream separation, drops show type I and

type II trajectories depending on other parameters of the flow. Note that for rigid particles in Stokes flow, the particles would not move out of the central plane. Increasing initial streamwise separation changes type I trajectory into type II due to increased overlap of the drop position with the zone of reversed streamlines. The terminal cross-stream separation for drops performing type I trajectory does not vary appreciably with initial separation.

## ACKNOWLEDGMENTS

K.S. acknowledges partial support from the NSF under Grant No. CBET-0625599. The authors thank an anonymous reviewer for pointing out the symmetry of the problem in a changed frame of reference, which led to substantial improvement in presentation of the results.

- <sup>1</sup>K. Sarkar and W. R. Schowalter, "Deformation of a two-dimensional drop at non-zero Reynolds number in time-periodic extensional flows: numerical simulation," *J. Fluid Mech.* **436**, 177 (2001).
- <sup>2</sup>K. Sarkar and W. R. Schowalter, "Deformation of a two-dimensional viscous drop in time-periodic extensional flows: analytical treatment," *J. Fluid Mech.* **436**, 207 (2001).
- <sup>3</sup>X. Y. Li and K. Sarkar, "Drop dynamics in an oscillating extensional flow at finite Reynolds numbers," *Phys. Fluids* **17**, 027103 (2005).
- <sup>4</sup>X. Y. Li and K. Sarkar, "Numerical investigation of the rheology of a dilute emulsion of drops in an oscillating extensional flow," *J. Non-Newtonian Fluid Mech.* **128**, 71 (2005).
- <sup>5</sup>K. Sarkar and W. R. Schowalter, "Deformation of a two-dimensional viscoelastic drop at non-zero Reynolds number in time-periodic extensional flows," *J. Non-Newtonian Fluid Mech.* **95**, 315 (2000).
- <sup>6</sup>X. Li and K. Sarkar, "Negative normal stress elasticity of emulsion of viscous drops at finite inertia," *Phys. Rev. Lett.* **95**, 256001 (2005).
- <sup>7</sup>X. Y. Li and K. Sarkar, "Effects of inertia on the rheology of a dilute emulsion of drops in shear," *J. Rheol.* **49**, 1377 (2005).
- <sup>8</sup>G. K. Batchelor and J. T. Green, "Hydrodynamic interaction of 2 small freely-moving spheres in a linear flow field," *J. Fluid Mech.* **56**, 375 (1972).
- <sup>9</sup>G. K. Batchelor and J. T. Green, "Determination of bulk stress in a suspension of spherical-particles to order C-2," *J. Fluid Mech.* **56**, 401 (1972).
- <sup>10</sup>C. I. Darabaner and E. Mason, "Particle motions in sheared suspensions XXII: interactions of rigid spheres (experimental)," *Rheol. Acta* **6**, 273 (1967).
- <sup>11</sup>N. A. Frankel and A. Acrivos, "Heat and Mass Transfer from Small Spheres and Cylinders Freely Suspended in Shear Flow," *Phys. Fluids* **11**, 1913 (1968).
- <sup>12</sup>C. R. Robertson and A. Acrivos, "Low Reynolds number shear flow past a rotating circular cylinder. 2. Heat transfer," *J. Fluid Mech.* **40**, 705 (1970).
- <sup>13</sup>G. Subramanian and D. L. Koch, "Centrifugal forces alter streamline topology and greatly enhance the rate of heat and mass transfer from neutrally buoyant particles to a shear flow," *Phys. Rev. Lett.* **96**, 134503 (2006).
- <sup>14</sup>G. Subramanian and D. L. Koch, "Inertial effects on the transfer of heat or mass from neutrally buoyant spheres in a steady linear velocity field," *Phys. Fluids* **18**, 073302 (2006).
- <sup>15</sup>D. R. Mikulencak and J. F. Morris, "Stationary shear flow around fixed and free bodies at finite Reynolds number," *J. Fluid Mech.* **520**, 215 (2004).
- <sup>16</sup>A. Acrivos, G. K. Batchelor, E. J. Hinch, D. L. Koch, and R. Mauri, "Longitudinal shear-induced diffusion of spheres in a dilute suspension," *J. Fluid Mech.* **240**, 651 (1992).
- <sup>17</sup>G. D. M. Mackay and S. G. Mason, "Particle motions in sheared suspensions. 15. Effects of diffusion on collision doublets of fluid drops," *Kolloid-Zeitschrift and Zeitschrift Fur Polymere* **195**, 138 (1964).
- <sup>18</sup>M. Loewenberg and E. J. Hinch, "Numerical simulation of a concentrated emulsion in shear flow," *J. Fluid Mech.* **321**, 395 (1996).
- <sup>19</sup>M. Loewenberg and E. J. Hinch, "Collision of two deformable drops in shear flow," *J. Fluid Mech.* **338**, 299 (1997).
- <sup>20</sup>R. Charles and C. Pozrikidis, "Significance of the dispersed-phase viscosity on the simple shear flow of suspensions of two-dimensional liquid drops," *J. Fluid Mech.* **365**, 205 (1998).
- <sup>21</sup>S. Guido and M. Simeone, "Binary collision of drops in simple shear flow by computer-assisted video optical microscopy," *J. Fluid Mech.* **357**, 1 (1998).
- <sup>22</sup>X. Y. Li and K. Sarkar, "Drop deformation and breakup in a vortex at finite inertia," *J. Fluid Mech.* **564**, 1 (2006).
- <sup>23</sup>P. M. Kulkarni and J. F. Morris, "Pair-sphere trajectories in finite-Reynolds-number shear flow," *J. Fluid Mech.* **596**, 413 (2008).
- <sup>24</sup>P. M. Kulkarni and J. F. Morris, "Suspension properties at finite Reynolds number from simulated shear flow," *Phys. Fluids* **20**, 040602 (2008).
- <sup>25</sup>C. J. Lin, J. H. Peery, and S. Wr, "Simple shear flow round a rigid sphere— inertial effects and suspension rheology," *J. Fluid Mech.* **44**, 1 (1970).
- <sup>26</sup>M. Zurita-Gotor, J. Blawdziewicz, and E. Wajnryb, "Swapping trajectories: A new wall-induced cross-streamline particle migration mechanism in a dilute suspension of spheres," *J. Fluid Mech.* **592**, 447 (2007).
- <sup>27</sup>I. E. Zarraga and D. T. Leighton, "Measurement of an unexpectedly large shear-induced self-diffusivity in a dilute suspension of spheres," *Phys. Fluids* **14**, 2194 (2002).
- <sup>28</sup>Y. G. Yan, J. F. Morris, and J. Koplik, "Hydrodynamic interaction of two particles in confined linear shear flow at finite Reynolds number," *Phys. Fluids* **19**, 113305 (2007).
- <sup>29</sup>S. K. Doddi and P. Bagchi, "Effect of inertia on the hydrodynamic interaction between two liquid capsules in simple shear flow," *Int. J. Multiphase Flow* **34**, 375 (2008).
- <sup>30</sup>E. Lac, A. Morel, and D. Barthes-Biesel, "Hydrodynamic interaction between two identical capsules in simple shear flow," *J. Fluid Mech.* **573**, 149 (2007).
- <sup>31</sup>E. Lac and D. Barthes-Biesel, "Pairwise interaction of capsules in simple shear flow: Three-dimensional effects," *Phys. Fluids* **20**, 040801 (2008).
- <sup>32</sup>G. Tryggvason, B. Bunner, A. Esmaeeli, D. Juric, N. Al-Rawahi, W. Tauber, J. Han, S. Nas, and Y. J. Jan, "A front-tracking method for the computations of multiphase flow," *J. Comput. Phys.* **169**, 708 (2001).
- <sup>33</sup>S. O. Unverdi and G. Tryggvason, "A front-tracking method for viscous, incompressible multi-fluid flows," *J. Comput. Phys.* **100**, 25 (1992).
- <sup>34</sup>G. I. Taylor, "The viscosity of a fluid containing small drops of another fluid," *Proc. R. Soc. London, Ser. A* **138**, 41 (1932).
- <sup>35</sup>G. I. Taylor, "The formation of emulsions in definable fields of flow," *Proc. R. Soc. London, Ser. A* **146**, 501 (1934).